

# A Noninvasive and Noncontact Jugular Venous Pulse Measurement Using a 60-GHz mmWave Sensor

*Shatabdi Das, Hadi Afsharan, Girish Dwivedi, and Omid Kavehei*

**Abstract** – The jugular venous pulse (JVP) offers key insights into right atrial pressure and cardiovascular health, but its assessment is often limited by anatomic variability and the invasiveness of catheterization. This study presents a noninvasive 60-GHz frequency-modulated continuous wave radar system for JVP estimation, using eigen beamforming to enhance signal quality and pulse detection. Optimized radar parameters enabled accurate capture of skin surface venous pulsations, validated through waveform comparison with simultaneous photoplethysmography. Signal localization within a direction of arrival range of  $-20^\circ$  to  $20^\circ$  confirmed system precision. Results highlight the radar’s potential for contactless, early-stage heart failure monitoring.

## 1. Introduction

Heart failure (HF) occurs when the heart fails to pump sufficient blood, leading to systemic congestion and impaired organ function. In Australia, HF accounts for 15% of hospitalizations, with more than 179,000 annual admissions costing approximately \$2.68 billion, a figure expected to rise with an aging population [1]. HF is classified into right and left-sided failure, with right heart failure contributing to venous congestion, a key factor in disease progression. The jugular venous pulse (JVP) serves as a crucial, noninvasive indicator of right heart function, reflecting changes in venous pressure and cardiac performance. Elevated JVP manifests as jugular venous distension, a visible sign of increased venous pressure [2].

The JVP waveform consists of distinct phases—‘a’, ‘c’, and ‘v’ waves—each corresponding to specific cardiac events, as shown in Figure 1. The internal jugular vein is the preferred site for JVP assessment because of its direct connection to proper atrial pressure. Understanding JVP dynamics enables clinicians to accurately diagnose the severity of right heart failure severity and

venous congestion, thereby reinforcing its role in cardiovascular monitoring.

Photoplethysmography (PPG) measures arterial blood flow and is strongly influenced by heart contractions (systole and diastole) [3]. Although both JVP and PPG provide different physiological insights, they are complementary signals related to cardiac cycles. Figure 1 illustrates the correlation between JVP and PPG waveforms, highlighting key cardiac cycle phases, where the ‘a’ wave precedes the PPG systolic peak, the ‘x’ descent aligns with the PPG rising phase, and the JVP ‘v’ wave corresponds to the PPG diastolic notch.

Traditional JVP monitoring is limited because of invasive methods, necessitating the development of noninvasive alternatives. Noninvasive approaches for JVP estimation have explored optical techniques; however, their reliability is often hindered by sensitivity to skin and tissue properties, which complicates calibration [4, 5]. Radar-based radio frequency sensing provides a more robust alternative for physiological monitoring, with previous studies employing 24-GHz microwave radar [6] and 900-MHz near-field radar [3] for detecting JVP. However, the lower spatial resolution of 900-MHz systems and phase variation issues in near-field configurations limit their effectiveness in capturing detailed JVP waveforms.

This study, for the first time, employs a 60-GHz frequency-modulated continuous wave (FMCW) radar for noncontact JVP assessment. The higher operating frequency provides enhanced spatial resolution and improved sensitivity to subtle surface displacements, making it well-suited for detecting the minute motion of the skin over the external jugular vein. The Infineon BGT60TR13C radar module was selected for its compact antenna-in-package design, reduced susceptibility to interference, and flexible signal configuration, making it ideal for biomedical radar sensing at close proximity.

Furthermore, this is the first study to incorporate electromagnetic simulations using the Sim4Life platform to assess the impact of radio frequency fields on the neck region in the context of JVP monitoring, ensuring safety compliance and verifying that radar signal interaction remains confined to superficial tissue layers.

## 2. System Design

The study uses a 60-GHz FMCW radar chipset (BGT60TR13C), an off-the-shelf, cost-effective sensor with one transmit and three receive antennas arranged

Manuscript received 18 February 2025.

Shatabdi Das and Omid Kaveheia are with the School of Biomedical Engineering, The University of Sydney, Sydney, NSW 2006, Australia; e-mail: shatabdi.das@sydney.edu.au, omid.kavehei@sydney.edu.au.

Hadi Afsharan and Girish Dwivedi are with the Department of Advanced Clinical and Translational Cardiovascular Imaging, Harry Perkins Institute of Medical Research, Murdoch, 5 Robin Warren Drive, Perth, WA 6150, Australia and the Department of Cardiology, Fiona Stanley Hospital, Murdoch, Perth, WA 6150, Australia; e-mail: hadi.afsharan@uwa.edu.au, girish.dwivedi@perkins.uwa.edu.au.

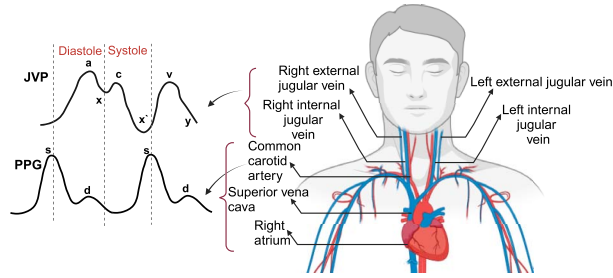


Figure 1. Interpretation of jugular venous pulse contour and PPG signal in a cardiac cycle (left). Schematic representation of the superficial venous system of the inferior anterior area of the neck, which connects the internal jugular vein (IJV) and external jugular vein (EJV) with the right atrium.

at right angles. This operates within the 58-GHz to 63-GHz range and allows customization of samples per chirp ( $N_s$ ), chirps per frame ( $N_c$ ), and chirp duration ( $T_c$ ). The receive and transmit antenna gains are 10 dBi and 6 dBi, respectively.

This high-sensitivity radar enables sub-millimeter motion detection, which is crucial for JVP measurement. Higher frequencies improve the detection of subtle movements due to their shorter wavelengths and enhanced phase sensitivity [7–9]. The 60-GHz system was chosen for its superior resolution in capturing JVP waveforms and small skin displacements.

Additionally, to assess electromagnetic interactions and safety, we employed the Sim4Life platform with the high-resolution Duke V3.0 voxel model, as shown in Figure 2 [10]. Specific absorption rate (SAR) and power density (PD) analysis at a higher frequency (35 GHz) confirmed that the energy is confined to superficial tissue layers (SAR: 1.01 W/kg; PD: 0.002 W/m<sup>2</sup> at a 2-mm depth), minimizing interference from deeper structures. This supports our focus on skin-surface displacements caused by JVP activity, as the radar primarily interacts with the outer tissue layers.

## 2.1 Radar Data Configuration

Radar data in each measurement frame are structured as a three-dimensional (3D) data cube in the time domain. The rows represent the number of receive antennas ( $N_{rx}$ ) per active transmit antenna, columns indicate chirps per frame ( $N_c$ ), and slices correspond to samples per chirp ( $N_s$ ). Each transmit-receive antenna pair forms a virtual antenna, and data are structured as ( $N_{rx} \times N_c \times N_s$ ) for signal processing, where samples per chirp define fast time and chirps per second define slow time.

## 2.2 Experimental Setup

Optimal radar placement is crucial for accurate JVP detection, as it balances signal strength to avoid saturation or loss of detail. The ideal neck position is between the collarbone and jawbone, with the subject angled between 30° and 45°, as venous return varies with posture.

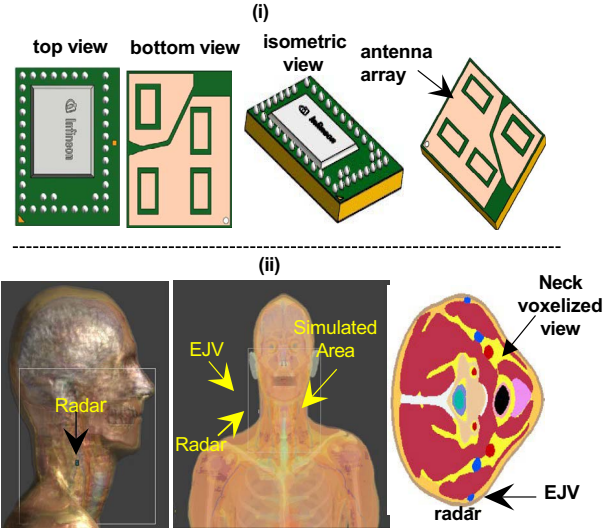


Figure 2. (a) Overview of FMCW radar simulation setup. (i) Sixty-GHz radar system with integrated-phased array antenna featuring one transmitter and three receivers. (ii) Radar positioning relative to the simulated area using a realistic human model (Duke).

To ensure precise measurements, the radar was updated to firmware v2.55, interfaced using Radar System Development Kit v3.3.0 (Infineon), and paired with MATLAB (2023a) for data analysis. Figure 3 illustrates a 3D-printed meshed cover ( $30 \times 10.5 \times 2 \text{ mm}^3$ ) provided stability during recordings. For the experiment, a single healthy subject (female, 26–30 years) was tested at four angles (0°, 30°, 45°, and 90°) with 30-second recording sessions. Finger PPG data (273 Hz sampling rate, 5-V supply) was collected for waveform comparison.

JVP signals, being low-amplitude venous pulsations, can be masked by breathing artifacts, making detection challenging. To address this, a JVP simulator using a speaker plate was developed to emulate venous pulsations. A synthesized beat signal with two tones (50 Hz, 54 Hz) was used to validate the signal processing methodology, following an approach inspired by previous research [11], as



Figure 3. (left) Indicative data recording setup. The radar sensor is placed near the jugular vein for data collection, while PPG data are collected using the finger PPG device. The subject is reclined on a base with a sensor placed in reasonable proximity to the neck at an almost 45° angle to monitor cardiovascular parameters. (right) The 3D-printed plastic case is nearly the size of a 1-dollar Australian coin.

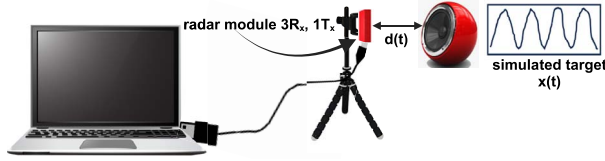


Figure 4. This setup features an experimental design replicating a patient target, with a speaker plate strategically oriented to face the radar system. The experiment involves synthesizing an audio signal meticulously composed of two specific frequencies, 50 Hz and 54 Hz, to evaluate the radar system’s response.

shown in Figure 4. The findings and impact of this experiment are discussed in Section 4.

### 3. Methodology: Signal Generation and Processing

Figure 5 represents the steps of signal generation and processing. The JVP detection process involves analyzing radar data structured as a 3D data cube with dimensions  $N_{rx} = 3$ ,  $N_c = 8$ , and  $N_s = 128$ , sampled at 1 MHz. A Fast Fourier Transform (FFT) is applied along the fast-time dimension to obtain a complex range profile, identifying the target within the detection area of the radar.

The signal processing workflow consists of several key steps. First, the raw data is reshaped and processed using FFT for each chirp and antenna. To improve signal quality, averaging is applied to reduce noise, and the inverse FFT is used to extract the In-phase (I) and quadrature (Q) complex signals for the two antennas (1 and 3) with the highest signal-to-noise ratio (SNR). Next, eigen beamforming [12, 13] is implemented to optimize signal reception while mitigating noise. The direction of arrival is estimated using eigenvector decomposition, enhancing signal clarity.

To extract physiological movements, phase variations from radar echoes are analyzed to track skin displacement. The displacement is computed as:

$$d_{skin} = \hat{\theta}_{skin} \times \frac{\lambda}{4\pi}$$

A bandpass filter (0.75–4 Hz) and a bandstop filter (0.9–1.1 Hz) are applied to mitigate arterial signal interference while preserving JVP characteristics. A correlation-based method is employed to identify and select the most accurate JVP pulses for analysis. The final processed signal effectively captures JVP variations, providing valuable insights for cardiovascular assessment and monitoring.

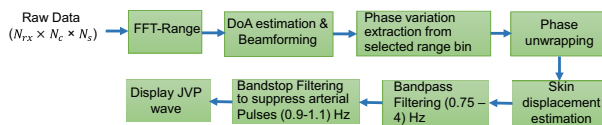


Figure 5. Schematic representation of the data processing sequence. After reshaping the raw data, an FFT is performed on the samples to obtain the range information. Upon computation of FFT, displacement is calculated from the phase variation, which is then used to extract the JVP.

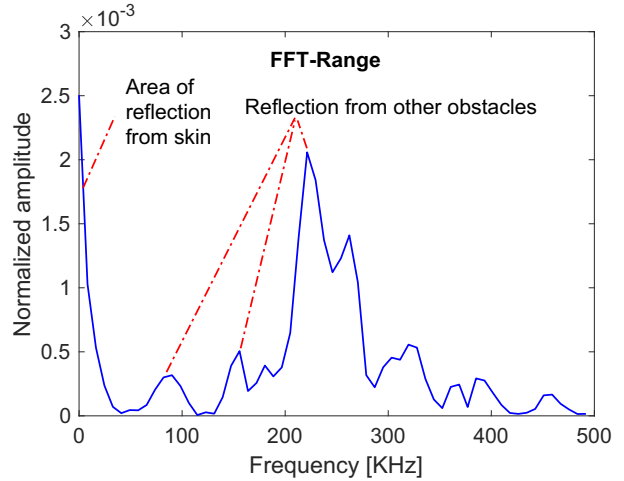


Figure 6. FFT range analysis shows the normalized amplitude of the radar signal across different frequency bins. The first peak corresponds to the reflection from the skin, while the following peaks indicate reflections from other environmental obstacles.

### 4. Results and Discussion

Antenna selection in this experiment was based on the SNR, which depends on the positioning of antennas relative to the vein. The optimal configuration places the vein equidistant between the selected antennas to maximize signal capture. As shown in Figure 6, the first FFT-range bin represents the initial radar reflection from the skin, while subsequent bins correspond to reflections from other environmental obstacles.

Our study investigates a proof of concept for JVP detection by varying radar parameters, including the number of samples per chirp, the number of chirps per frame, and the sampling frequency. As higher sample counts per chirp enhance JVP visibility, in this setup, we used 128 samples/chirp, 8 chirps/frame, and a 1000-kHz sampling frequency, with a chirp duration of 132.987  $\mu$ s. Figure 7 presents the final extracted JVP waveform obtained at a body inclination of 45°, following the full signal processing pipeline outlined in Figure 5. The waveform exhibits

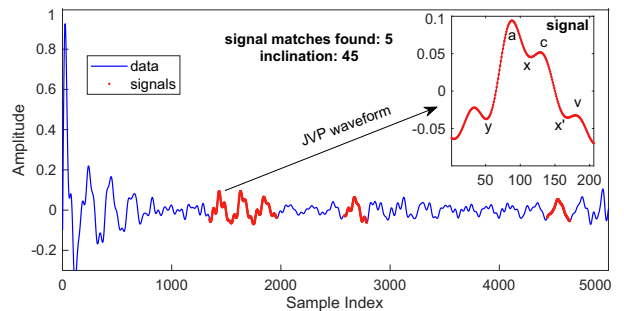


Figure 7. Detection of JVP waveforms in a signal. The main graph displays the overall data signal (blue) with detected JVP waveforms highlighted in red. Five signal matches were found. The inset (top right) zooms into a typical JVP waveform, marked from points ‘a’ to ‘x’ and ‘x’ to ‘v’, indicating the ascent and descent of the waveform, respectively.

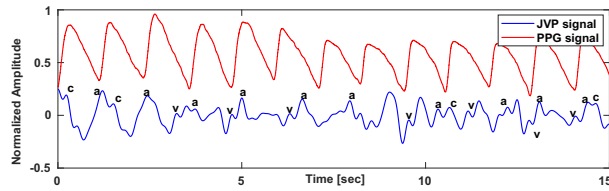


Figure 8. Comparative analysis of the JVP and the PPG signals obtained from a synchronized measurement. There is consistent timing between PPG peaks and specific JVP descents, such as the y-descent following atrial filling. This illustration highlights the temporal alignment and amplitude differences between the venous pulsations observed in the neck and the arterial pulsations measured peripherally.

clear morphological components of venous pulse dynamics, demonstrating the method's effectiveness in isolating venous signals and suppressing arterial interference.

Figure 8 presents the recorded JVP and PPG signals simultaneously from the same subject, while PPG was collected using a fingertip optical sensor and JVP from the neck at an inclined position. A synchronized measurement approach was used, aligning both signals based on their standard frequency components. As both signals reflect cardiac cycles, they typically overlap in the (0.8-2) Hz range, with a common frequency of 1.13 Hz in this experiment. The PPG rising peaks generally coincide with JVP descents, though this alignment may vary because of respiratory influences, venous return timing, and physiological conditions. This serves as a qualitative, physiological cross-reference to support the correct identification of waveform components in the radar-extracted JVP signal.

Figure 9 presents the JVP signals in the time domain. Figure 10 shows their frequency spectrum at the following three inclination angles:  $0^\circ$ ,  $45^\circ$ , and  $90^\circ$ . These signals illustrate the impact of posture on JVP visibility.

At  $0^\circ$  (lying flat), venous return increases, causing the carotid arterial pulse to dominate and overshadow the JVP signal. Higher amplitudes in Figure 9 indicate JVP interference from arterial pulsation. Peaks near 0 Hz in the frequency spectrum reflect slow venous return influenced by gravity. At  $45^\circ$ , the spectral peaks

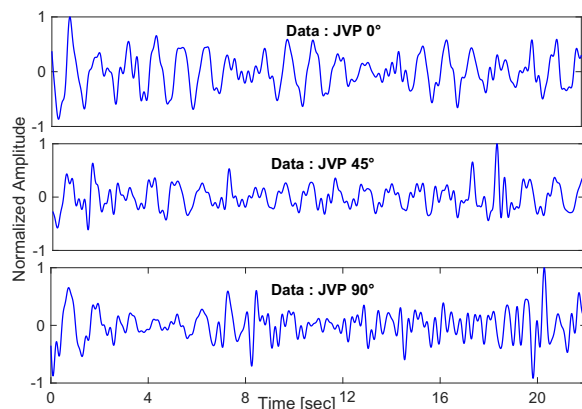


Figure 9. Time domain representation of the JVP signal at different inclination angles ( $0^\circ$ ,  $45^\circ$ , and  $90^\circ$ ), illustrating variations in waveform morphology with posture.

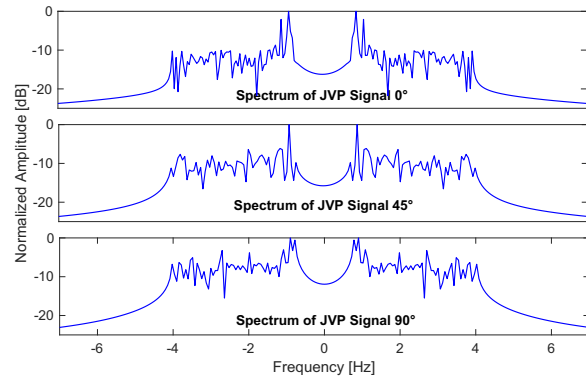


Figure 10. Frequency domain representation of the JVP signal at different inclination angles ( $0^\circ$ ,  $45^\circ$ , and  $90^\circ$ ), showing spectral energy distribution and the effect of posture on signal frequency components.

shift, and JVP pulses appear more distinct as this angle balances gravitational effects. At  $90^\circ$  (upright), venous return decreases due to gravity, resulting in a weaker JVP signal with an overall spectral energy shift, making interpretation more challenging.

Thus,  $45^\circ$  is the optimal angle for stable and reliable JVP measurement, minimizing interference while preserving signal clarity.

Our experiment confirms the feasibility of 60-GHz FMCW radar for noninvasive JVP extraction, using its high resolution and sensitivity to detect subtle skin movements. Optimized parameters include 128 samples per chirp, a 250-Hz frame rate, at least 8 chirps per frame, and a 0.00013-second chirp duration. Shorter chirp durations prevent interference, while longer durations require increased radar-skin distance and receiver gain adjustments. The radar receiver, with a single in-phase mixer, produces a real-valued Intermediate Frequency (IF) signal processed via Fourier transform to extract complex components. Compared with IQ radar, this architecture exhibits phase variation-induced fading, which impacts signal stability. As illustrated in Figure 11, quadrature radar receivers offer significant improvements

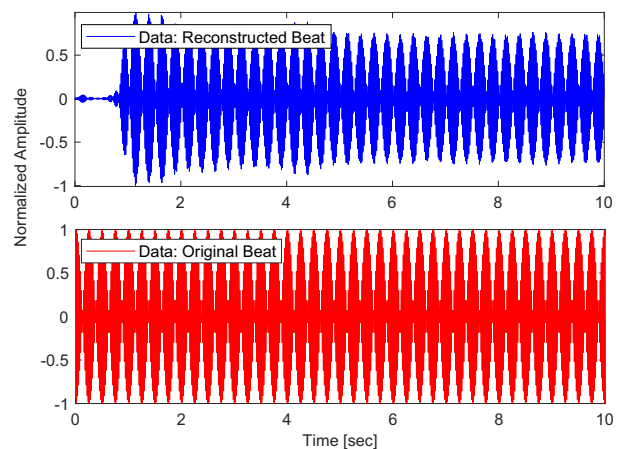


Figure 11. (Top) Beat signal reconstructed by radar. (Bottom) The original signal was played on the speaker.

over nonquadrature receivers, enhancing JVP detection accuracy. This was achieved through the experiment mentioned in Figure 4.

Optimal radar placement (2 mm) was crucial to avoid signal distortion. Key optimizations included a higher sampling rate, suppressed averaging, and antenna selection for improved SNR. Despite hardware limits, 60-GHz radar shows promise for JVP monitoring.

## 5. Conclusion

This study investigates the feasibility of a 60-GHz FMCW radar for noninvasive JVP measurement, highlighting its potential as a cost-effective alternative to traditional methods. While promising, further clinical validation is necessary to compare results with a gold-standard baseline. Our ongoing efforts focus on collecting clinical data, improving signal quality, and integrating automated signal processing. Despite hardware limitations, we successfully measured millimeter-scale JVP variations, analyzed the effects of body inclination, and compared the results with finger PPG as a physiological cross-reference. Physiological differences across individuals may alter radar signal behavior, underscoring the importance of accounting for tissue variability in future validation efforts. Our future research will expand on these findings with a larger cohort. This technology could become a valuable tool for early detection of heart failure and reducing hospital admissions.

## 6. References

1. Australian Institute of Health and Welfare, "Heart, Stroke and Vascular Disease: Australian Facts, Atrial Fibrillation," <https://shorturl.at/bnRRb> (Accessed 28 May 2024).
2. T. B. Conroy, J. Zhou, and E. C. Kan, "Jugular Venous Pulse Waveform Extraction From a Wearable Radio Frequency Sensor," *IEEE Sensors Journal*, **23**, 9, 2023, pp. 10140-10148.
3. J. E. Johnson, O. Shay, C. Kim, and C. Liao C, "Wearable Millimetre-Wave Device for Contactless Measurement of Arterial Pulses," *IEEE Transactions on Biomedical Circuits and Systems*, **13**, 6, December 2019, pp. 1525-1534.
4. I. García-López and E. Rodríguez-Villegas. Extracting the Jugular Venous Pulse From Anterior Neck Contact Photo-plethysmography. *Scientific Reports*. **10**, 1, February 2020, p. 3466.
5. S. McGee, *Evidence-Based Physical Diagnosis*. Cambridge, UK: Elsevier Health Sciences; 2021.
6. A. G. Vinayak, J. Levitt, B. Gehlbach, A. S. Pohlman, J. B. Hall, et al., "Usefulness of the External Jugular Vein Examination in Detecting Abnormal Central Venous Pressure in Critically Ill Patients," *Archives of Internal Medicine*, **166**, 19, October 2006, pp. 2132-2137.
7. N. Vysotskaya, C. Will, L. Servadei, N. Maul, C. Mandl C, et al., 2023. Continuous Non-Invasive Blood Pressure Measurement Using 60 GHz-Radar—A Feasibility Study. *Sensors*, **23**, 8, April 2023, p. 4111.
8. M. Arsalan, A. Santra, and C. Will, "Improved Contactless Heartbeat Estimation in FMCW Radar via Kalman Filter Tracking," *IEEE Sensors Letters*, **4**, 5, 2022, pp. 1-4.
9. A. Ahmad, J. C. Roh, D. Wang, and A. Dubey, "Vital Signs Monitoring of Multiple People Using a FMCW Millimeter-Wave Sensor," 2018 IEEE Radar Conference, Oklahoma City, OK, April 23–27, 2018, pp. 1450-1455.
10. ZMT Zurich MedTech AG, "Sim4Life Computational Platform," <https://www.sim4life.com> (Accessed 25 February).
11. W. Hu, Z. Zhao, Y. Wang, H. Zhang, and F. Lin, "Noncontact Accurate Measurement of Cardiopulmonary Activity Using a Compact Quadrature Doppler Radar Sensor," *IEEE Transactions on Biomedical Engineering*, **61**, 3, 2013, pp. 725-735.
12. D. D. Feldman and L. J. Griffiths, "A Projection Approach for Robust Adaptive Beamforming," *IEEE Transactions Signal Processing*, **42**, 4, 1994, pp. 867-876. See doi: 10.1109/78.285650.
13. C. Fonteneau, M. Crussière, and B. Jahan, "An Efficient Analog Eigen-Beamforming Procedure for Wideband mmWave MIMO-OFDM Systems," 2022 IEEE 23rd International Symposium on a World of Wireless, Mobile and Multimedia Networks (WoWMoM), Belfast, UK, June 14–17, 2022.